This is a repository copy of *Composite porous scaffold of PEG/PLA support improved bone matrix deposition in vitro compared to PLA-only scaffolds*.

White Rose Research Online URL for this paper:
http://eprints.whiterose.ac.uk/126492/

Version: Accepted Version

Article:

Composite porous scaffold of Polyethylene glycol (PEG)/ Polylactic acid (PLA) support improved bone matrix deposition *in vitro* compared to PLA -only scaffolds

Birru Bhaskar[1, 2], Robert Owen[2], Hossein Bahmaee[2,3], Zena Wally[2], Parcha Sreenivasa Rao[1, **], Gwendolen C Reilly[2, *] 🆔

[1]Department of Biotechnology, National Institute of Technology Warangal, Telangana, India- 506004

[2] Department of Materials Science and Engineering, University of Sheffield, INSIGNEO Institute for in silico medicine, The Pam Liversidge Building, Sir Frederick Mappin Building, Mappin Street, Sheffield, S1 3JD, United Kingdom

[3]Department of Materials Science and Engineering, University of Sheffield, The Kroto Research Institute, North Campus, Broad Lane, Sheffield, S3 7HQ, United Kingdom.

Corresponding author: Dr. Parcha Sreenivasa Rao, parcha@nitw.ac.in

Co-corresponding author: Dr. Gwendolen C Reilly, g.reilly@sheffield.ac.uk

Abstract:

Controllable pore size and architecture are essential properties for tissue-engineering scaffolds to support cell ingrowth colonization. To investigate the effect of PEG addition on porosity and bone-cell behavior, porous Polylactic acid (PLA)-Polyethylene glycol (PEG) scaffolds were developed with varied weight ratios of PLA-PEG (100/0, 90/10, 75/25) using solvent casting and porogen leaching. Sugar 200-300 μm in size was used as a porogen. To assess their suitability for bone tissue engineering, MLO-A5 murine osteoblast cells were cultured and cell metabolic activity, alkaline phosphatase (ALP) activity and bone-matrix production determined (alizarin red S staining for calcium, direct red 80 staining for collagen). It was found that metabolic activity was significantly higher over time on scaffolds containing PEG, ALP activity and mineralized matrix production were also significantly higher on scaffolds containing 25% PEG. Porous architecture and cell distribution and penetration into the scaffold were analyzed using SEM and confocal microscopy, revealing that inclusion of PEG increased pore interconnectivity and therefore cell ingrowth in comparison to pure PLA scaffolds. The results of this study confirmed that PLA-PEG porous scaffolds support mineralizing osteoblasts better than pure PLA scaffolds, indicating they have a high potential for use in bone tissue engineering applications.

Key words: Polylactic acid (PLA), Polyethene glycol (PEG), Bone tissue engineering, MLO-A5, porosity.

1. Introduction:

Bone tissue engineering aims to combine scaffolds, osteoblasts and physiochemical factors to regenerate healthy bone tissue. The scaffold material plays a vital role in the development of engineered bone, and it should possess a highly porous structure that promotes cell attachment, proliferation and bone tissue formation and mineralization [1]. Synthetic and natural polymeric scaffolds can be used as a bone tissue-engineering scaffold. The advantage of synthetic polymer scaffolds is their customizable chemical, physical and mechanical properties. Many biocompatible and biodegradable synthetic scaffolds have been developed for bone tissue engineering applications, such as polylactic acid (PLA), poly lactide-co-glycolide (PLGA), polycaprolactone (PCL) and polyurethane (PU) [2]–[4]. Porogen and polymer composition determine the nature of the porous structure of the scaffolds; for example pore size, shape and interconectivity. The porosity of the scaffold facilitates cell migration, ingrowth, and effective nutrient distribution and waste removal. Therefore, appropriate scaffold porosity is essential for successful tissue engineering. Numerous methods have been developed to introduce porosity into scaffold materials, including solvent casting-particulate leaching [5], supercritical CO_2 gas foaming and particulate leaching [6], emulsion freezing/freeze-drying [7], and emulsion templating [8]. The solvent casting-particulate leaching technique is widely accepted as a simple, cost-effective method to provide a porous architecture within the scaffold [9]. Sodium chloride, ammonium bicarbonate, and glucose with different crystal sizes have all been used as porogens to fabricate porous scaffolds, and the porosity of scaffold can be controlled by the amount and dimensions of the porogen [10]–[13].

Inclusion of PLA is an excellent way of modifying the mechanical properties and the degradation rate when developing biomaterials for specific applications. PEG is also an effective modifier, as it is non-toxic and biocompatibile [14]–[16]. Due to its solubility in

water, the degradation can be controlled for different biomedical applications. For tissue engineering, degradation rate is a vital parameter as it should match the rate of tissue formation, therefore; in the current study PEG is used to develop porous PLA/PEG scaffolds. It has previously been shown that the degradation rate of PLA/PEG scaffolds is enhanced with increasing PEG content [10].

MLO-A5 are an immortal clonal murine osteoblast cell line capable of rapidly depositing mineralised extracellular matrix in sheets rather than nodules [17]. They have very high ALP activity and expression of bone sialoprotein and osteocalcin, all hallmarks of the post-osteoblast phenotype [18]. Due to their high rate of bone matrix production in comparison to other murine bone cell lines, such as MC3T3-E1, they have been used extensively for studying bone cell behaviour and assessing bone tissue engineering scaffolds [1], [19], [20].

Previous studies have reported on the degradation and mechanical properties of PLA-PEG scaffolds [10], [21] and it was reported that addition of PEG to PLA changed the crystallization and the rheological behavior of the matrix, decreased T_g, facilitated the spherullitic growth (growth of spherical crystalline regions), reduced the elastic and viscous behavior and enhanced crystallization properties to increase the open-pore and pore density. However, little is known about the ability of such scaffolds to support bone cell growth. Therefore, in this study, we synthesized solvent cast/porogen leached polylactic acid (PLA)-poly ethylene glycol (PEG) porous scaffolds and varied the overall porosity by modulating the PEG: PLA ratio. We evaluated the morphological variation and cell penetration of different PLA-PEG scaffolds and tested the compatibility and ability to support bone matrix deposition using MLO-A5 osteoblastic cells.

2. Materials and Methods:

2.1. Materials

Polylactic acid (PLA4042D) (NatureWorks®, USA), Polyethylene glycol (PEG4000), Dichloromethane (Fisher Chemicals, UK), α-minimal expansion media (α-MEM) (Lonza, UK), Fetal Bovine serum (FBS), Penicillin-Streptomycin-Glutamine (PSG), Resazurin Red Salt, Alkaline phosphatase kit (Thermo Fisher Scientific, UK), Alizarin Red S Salt, Direct Red 80. All chemicals and reagents were obtained from Sigma-Aldrich, UK unless otherwise stated.

2.2. Porous scaffold fabrication using Solvent casting-porogen leaching

Different weight ratios of PLA and PEG (100/0, 90/10 and 75/25 weight %) were dissolved in dichloromethane. Polymer solutions were mixed with caster sugar (Tesco PLC, UK) (200-300 μm) in the weight/weight ratio of 1:9 and poured into Petri dishes for solvent evaporation for 48 h in a fume cupboard before using a vacuum to remove the remaining solvent. To leach the sugar particles scaffolds were immersed in diH$_2$O for 72 h with the water replaced every 6 h. Scaffolds were then dried under vacuum for 48 h. Circular disks of diameter 1 cm were cut using a laser cutter (Mini 19 Laser, Epilog Laser, UK) for cell culture studies. In this study, 100% of PLA, 90/10- PLA/PEG, and 75/25-PLA/PEG are represented as PLA100, PLA90 and PLA75 respectively.

2.3. MLO-A5 cell culture on PLA-PEG scaffold

Scaffolds were sterilized by immersion in 70% ethanol for two days and then washed thrice with sterile PBS before submerging in basal media (BM) (α-MEM, 10% FBS, 1% PSG) for two days to allow proteins to adsorb to the surface to improve cell attachment. Then, 2×10^4

MLO-A5 (Kindly donated by Dr. Lynda Bonewald, University of Missouri) cells of passage number 52 were seeded on each scaffold (Scaffold size; diameter ×thickness=10mm×4mm) and left for 2 h before submerging in 2 mL of BM and incubating overnight. Scaffolds were transferred to a 12 well plate on day 1 so that only cells attached to the scaffold were cultured, and were maintained in supplemented media (BM + 5 mM β-glycerolphosphate (βGP), 50 µg/mL ascorbic acid-2-phosphate (AA-2P) to facilitate bone matrix production for the remainder of the experiment. The media was exchanged every 2-3 days.

2.4. Resazurin Reduction (RR) Assay

Cell metabolic activity was elucidated by RR assay and used to estimate cell number. Scaffolds were transferred to new well plates and 2mL of RR working solution (10 vol% of RR stock solution (1 mM resazurin sodium salt in diH2O) in BM) was added before incubating for 4 h. Seeding wells were also assayed to determine seeding efficiency. 200 µL of the reduced working solution was transferred to a clear 96 well plate and fluorescence readings at excitation wavelength 540 nm, and emission wavelength 590 nm (Tecan infinite 200-pro) were taken. Excess working solution was removed and the samples were washed twice with PBS to remove residual working solution trapped within the scaffold before adding fresh media.

2.5 Alkaline Phosphatase activity (ALP)

Culture media was removed from the scaffolds which were then washed twice with PBS. Scaffolds were transferred to 1.5 mL tubes and 1 mL of cell digestion buffer (10 v/v% cell assay buffer (1.5 M Tris–HCl, 1 mM $ZnCl_2$, 1 mM $MgCl_2$ in deionized water (diH$_2$O), 1% TritonX100, in diH$_2$O)) was added and incubated for 30 min before storing at 4 °C overnight. Samples were vortexed for 15 seconds and a freeze-thaw cycle was performed three times (-

80 °C 10 min, 37 °C 15 min) to facilitate cell digestion by ice crystal formation. Finally, samples were centrifuged at 10,000 rpm for 5 min.

180 μL of PNPP Phosphatase Substrate (Thermo Scientific, UK) was added in a clear 96 well plate and combined with 20 μL cell lysate. The well plate was then immediately added to the plate reader and absorbance readings were taken at a wavelength of 405 nm every minute for 30 min. ALP activity was expressed as nmol of p-nitrophenol per minute (nmol pNP/min), assuming that one absorbance value equals 19.75 nmol of the product.

2.6. DNA assay

The amount of double standard DNA is an indicator of cell number, which can be calculated using the quant-iT™ dsDNA assay kit (Thermo Scientific, UK). 10 μL of cell lysate was combined with 90 μL of working solution in an opaque well plate, wrapped in well plate and incubated at room temperature for 10 min to allow the DNA and dye to conjugate. Fluorescence readings were taken at an excitation wavelength of 485 nm and an emission wavelength of 535 nm. Fluorescence values were converted to ng of DNA with a standard curve.

2.7 Formaldehyde fixation

Scaffolds were fixed prior to Alizarin Red S (ARS) and DR80 staining and confocal imaging. Fixing was performed by removing the culture media and washing twice with PBS. Samples were then submerged in 3.7% formaldehyde for 30 minutes before rinsing a further two times in PBS. Samples were stored at 4 °C in PBS until use.

2.8. Alizarin Red S Staining assay (ARS)

Calcium deposition by the cells was measured using Alizarin Red S. The samples were washed twice with diH$_2$O, and then 2mL of ARS working solution (1 w/v% ARS dissolved in diH$_2$O) was added to each scaffold, incubated for 30 min. ARS solution was removed and

they were washed with diH_2O every five minutes with gentle orbital shaking, continued until the water remained clear. 5% of perchloric acid was added to each sample to destain the samples, left for 15 min with gentle orbital shaking. 150 µL of destained solution was taken to measure the absorbance readings at a wavelength of 405 nm. These absorbance values were converted to concentration of ARS ((µg/mL) using standard curve.

2.9. Direct Red 80 Staining Assay (DR80)

Total collagen content was detected by using DR80 assay. The samples were washed thrice with water after performing the ARS assay and then 2 mL of DR80 working solution (1 w/v% direct red 80 in saturated picric acid) was added to each sample, then left for 18h with orbital shaking at 100 rpm. 0.2 M sodium hydroxide: methanol (1:1) was added to destain the samples and left for 20 min with orbital shaking at 100 rpm. The absorbance of 150 µL of destained solution was measured using a plate reader at 405 nm. The DR80 concentration was (µg/mL) calculated using a standard curve.

2.10. Confocal Imaging

To prepare fixed samples for imaging they were immersed in Immunocytochemistry (ICC) buffer (1% BSA, 0.1% Triton X-100 in PBS) for 20 min. Scaffolds were submerged in 0.2% Propidium Iodide (PI) and 1% Phalloidin FITC (1:1000 in ICC buffer) working solution and wrapped in foil, for 3h. The stain was removed from the sample and washed with PBS. Samples were stored wrapped foil at 4 °C in PBS until use.

Confocal images (512 x 512 pixels) were obtained using a Zeiss LSM 510Meta upright confocal microscope with 10x objective (EC Plan-Neofluar 10X/0.30, Carl Zeiss Ltd, UK), with a pixel dwell time of 2.56 µs. Propidium Iodide (PI) was excited using a laser wavelength of 543 nm and Phalloidin-FITC detected using a wavelength 488 nm. Scaffold 3D images were produced using Z-stacking, with 35 images taken at 6.4 µm.

2.10. Scanning electron microscopic images

Scanning electron microscopy (SEM) was used to examine the porosity and cell penetration into PLA-PEG scaffolds. To prepare seeded samples for imaging, fixed scaffolds were submerged in 1 vol% osmium tetroxide in PBS at room temperature for 2 hours before sequential dehydration in graded ethanol (50, 70, 80, 90, 100, 100 vol%) for ten minutes at each step. Finally, samples were immersed in 100% Hexamethyldisilane (HMDS) for three minutes before leaving to air dry for 3 days.

To image, all samples were mounted on a carbon tab, sputter coated with gold, then imaged using a Philips XL 30S FEG with an electron beam with an energy of 20 kV. Images were analyzed using the measurement tool in Image J.

2.11. Porosity Distribution anaysis

Image J software was used to analyse the overall porosity distribution of the scaffold. 50 pores were randomly choosen from each scaffold SEM image and three scaffolds per each condition considered. The results were represented in Mean±SD of three samples per each condition.

2.12 Statistical Analysis

Statistical analysis was performed using Graphpad prism 7.0 software. All the experiments were conducted two times with three samples for each condition (n=6). The results are presented as Mean±SD and two-way ANOVA and one-way ANOVA were used to evaluate the statistical significance with Tukey's post- hoc test for multiple comparisons.

3. Results and Discussion

3.1. Metabolic activity of MLO-A5 cells

On day 1, there was no significant difference in cell viability between PEG containing and pure PLA scaffolds. Similarly, by comparing the ratio of cell metabolic activity on the scaffolds to the seeding wells, there was no significant difference in seeding efficiency. The metabolic activity on all scaffolds increased over time indicating that cell proliferation was supported. By day 14 and 21 cell viability was significantly higher in the PEG containing scaffolds than the pure PLA scaffolds ($p < 0.01$) (Fig. 1B) indicating that PEG containing scaffolds provided favorable conditions for cell growth and colonization.

3.2. ALP, ARS and DR80 assays

ALP and DNA quantification assays were performed on day 14. Normalized ALP activity was significantly higher on PLA75 scaffolds than PLA90 and PLA100 scaffolds (Fig. 2A, $p < 0.001$). There was no difference between PLA100 and PLA90 scaffolds. Calcium deposition on day 21 was significantly higher on PLA75 scaffolds in comparison to PLA100 and PLA90 (Fig. 2B, $p < 0.01$). As with ALP, there was no significant difference between PLA100 and PLA90 calcium deposition as assayed on day 21 by ARS quantification. Both PEG containing scaffolds supported significantly higher collagen deposition that the pure PLA scaffold (Fig. 2C $p < 0.05$), although there was no significant difference between the

PLA90 and PLA75 compositions. Overall, it can be seen that the inclusion of PEG has improved the osteogenic performance of these scaffolds, with PLA75 having the greatest positive effect on ALP activity and mineralized extracellular matrix production (ECM).

Cell-biomaterial interaction is crucial as cells seeded into the scaffold have to maintain their phenotype, have a favorable cell–matrix interaction, and secrete large amounts of ECM. To facilitate this, the biomaterial must support cell attachment and proliferation [22]. In the current study, MLO-A5 cells' proliferation throughout the scaffolds was confirmed by increasing metabolic activity over time. Proliferation was improved on PEG containing scaffolds, which enabled higher mineralization and collagen formation (Fig. 2). These results confirm that PLA-PEG scaffolds are highly compatible with this osteoblast cell line and support high levels of bone matrix formation, demonstrating their potential for bone tissue engineering.

3.3. SEM images

SEM images were used to assess the porosity of scaffolds. The top and cross-sectional views indicated there were pores throughout all the scaffolds (Fig. 3A). Larger pores were observed in the cross-sectional SEM images of PEG containing scaffolds (PLA75 and PLA90). The overall pore size distribution in all scaffold compositions is given in Fig. 3C. It can be seen that in the PLA75 composition, the inclusion of PEG has resulted in a smaller proportion of small pores (0-100 μm, $p<0.01$) and a greater proportion of larger pores (200-300 μm, $p<0.01$). This indicates that inclusion of PEG alters the pore size distribution by favoring the formation of larger pores. As the porosity introduced by the porogen is the same for all polymer blends, these larger pores appear to form during the leaching stage by the merging of smaller pores. A potential mechanism for this is the rupture of thin polymer walls surrounding the pores that form as the solvent evaporates during the casting stage [23]. As

PEG is more hydrophilic than PLA, swells in water and is water soluble, when PEG content is increased, more of these thin walls rupture during leaching resulting in more large pores being formed [24], [25]. To assess how successfully cells penetrated into the porous network of the scaffolds, the cell seeded scaffolds were examined by SEM on day 7 (Fig. 3B). Cells were visible within all scaffold types and could be see covering the internal pores in cross-sectional images.

A similar method has previously been used to develop 3D scaffolds, which had high porosity, and controllable macropore size and wall morphology [26]. Porosity facilitates cell ingrowth and colonization of the scaffold, which is one of the most important considerations for tissue engineering [8], [10], [27]. The porosity of PLA/PEG/NaCl scaffolds has been reported to reach as high as 80% with high pore density and open-pore structure [27]. Here we demonstrated that this improved porosity is beneficial for long term cell growth of osteblastic bone cells. The MLO-A5 cells proliferated on the scaffolds and cells migrated through the pores across the scaffold and were well distributed, as confirmed by cross-sectional SEM images of cells on day 7 of culture.

3.4. Confocal microscopy

The penetration of MLO-A5 cells into the scaffold and can be observed using Z-stack confocal images with a depth of 224 μm. Cell nuclei are displayed as red and actin as green (Fig. 4). In the controls, there are no cells hence they appear black as no autofluorescence was observed for any scaffold composition. The porous structure allowed cells to migrate into the internal network of the thick scaffold. Cell-cell interaction, nutrient transport, removal of biological waste from within the scaffold and the cell seeding efficiency are all affected by porosity of the scaffold. The correct porosity range is important, as cell penetration into the scaffold could be prevented by very small pores and very large pores are not favorable for

cell adhesion due to the reduced area for cells to colonize [28]–[30]. In the present study, we have observed that cells were well distributed over the scaffold and penetrated into the scaffold.

4. Conclusion

In this study, we developed 3D porous PLA-PEG scaffolds using solvent casting-porogen leaching. We have observed that PEG improved the porous structure by altering the pore size distribution to increase pore size without increasing total porosity. MLO-A5 cells were cultured on these PLA-PEG scaffolds to investigate the effect of PEG incorporation on cell proliferation and bone matrix formation. Initial cell attachment was not affected by the addition of PEG to PLA despite the effect on pore size distribution, but it was observed that scaffolds containing PEG supported greater metabolic activity enhanced over time, indicating a higher cell number. Cell ingrowth is crucial for a successful tissue-engineered bone scaffold, and this was observed here by SEM images and confocal imaging showing excellent cell migration into the scaffold. ALP activity and mineralized matrix production was significantly increased in the composite scaffolds containing the highest ratio of PEG (PLA75). The present study suggests that PLA-PEG scaffolds could have major applications in bone tissue engineering and that PEG can be incorporated to improve osteogenic behavior.

References

[1]   G. Tetteh, A. S. Khan, R. M. Delaine-Smith, G. C. Reilly, and I. U. Rehman, "Electrospun polyurethane/hydroxyapatite bioactive Scaffolds for bone tissue engineering: The role of solvent and hydroxyapatite particles," *J. Mech. Behav. Biomed. Mater.*, vol. 39, pp. 95–110, 2014.

[2]   S. Puwanun, F. J. Bye, M. M. Ireland, S. MacNeil, G. C. Reilly, and N. H. Green, "Production and characterization of a novel, electrospun, tri-layer polycaprolactone membrane for the segregated co-culture of bone and soft tissue," *Polymers (Basel).*, vol. 8, no. 6, pp. 1–9, 2016.

[3]   N. . Mekala, R. R. Baadhe, and P. S. Rao, "Study on osteoblast like behavior of umbilical cord blood cells on various combinations of PLGA scaffolds prepared by salt fusion," *Curr. Stem Cell Res. Ther.*, vol. 8, no. 3, pp. 253–259, 2013.

[4]   S. A. Guelcher, "Biodegradable Polyurethanes: Synthesis and Applications in Regenerative Medicine," *Tissue Eng. Part B Rev.*, vol. 14, no. 1, pp. 3–17, 2008.

[5]   W. L. Murphy, R. G. Dennis, J. L. Kileny, and D. J. Mooney, "Salt Fusion: An

Approach to Improve Pore Interconnectivity within Tissue Engineering Scaffolds," *Tissue Eng.*, vol. 8, no. 1, pp. 43–52, 2002.

[6] B. Chen, X. Jing, H. Mi, H. Zhao, W. Zhang, X. Peng, and L. Turng, "Fabrication of Polylactic Acid/Polyethylene Glycol (PLA/PEG) Porous Scaffold by Supercritical CO_2 Foaming and Particle Leaching," *Polym. Eng. Sci.*, vol. 55, no. 6, pp. 1339–1348, 2015.

[7] N. Sultana and M. Wang, "PHBV/PLLA-based composite scaffolds fabricated using an emulsion freezing/freeze-drying technique for bone tissue engineering: surface modification and in vitro biological evaluation," *Biofabrication*, vol. 4, no. 1, p. 15003, 2012.

[8] R. Owen, C. Sherborne, T. Paterson, N. H. Green, G. C. Reilly, and F. Claeyssens, "Emulsion Templated Scaffolds with Tunable Mechanical Properties for Bone Tissue Engineering," *J. Mech. Behav. Biomed. Mater.*, vol. 54, pp. 159–172, 2015.

[9] K. F. Leong, C. M. Cheah, and C. K. Chua, "Solid freeform fabrication of three-dimensional scaffolds for engineering replacement tissues and organs," *Biomaterials*, vol. 24, no. 13, pp. 2363–2378, 2003.

[10] T. Serra, M. Ortiz-Hernandez, E. Engel, J. A. Planell, and M. Navarro, "Relevance of PEG in PLA-based blends for tissue engineering 3D-printed scaffolds," *Mater. Sci. Eng. C*, vol. 38, no. 1, pp. 55–62, 2014.

[11] N. Thadavirul, P. Pavasant, and P. Supaphol, "Development of polycaprolactone porous scaffolds by combining solvent casting, particulate leaching, and polymer leaching techniques for bone tissue engineering," *J. Biomed. Mater. Res. - Part A*, vol. 102, no. 10, pp. 3379–3392, 2014.

[12] S. Taherkhani and F. Moztarzadeh, "Fabrication of a poly(ε-caprolactone)/starch nanocomposite scaffold with a solvent-casting/salt-leaching technique for bone tissue

engineering applications," *J. Appl. Polym. Sci.*, vol. 133, no. 23, pp. 19–21, 2016.

[13] M. Shin, H. Abukawa, M. J. Troulis, and J. P. Vacanti, "Development of a biodegradable scaffold with interconnected pores by heat fusion and its application to bone tissue engineering," *J. Biomed. Mater. Res. Part A*, vol. 84A, no. 3, pp. 702–709, 2008.

[14] R. Huang, X. Zhu, T. Zhao, and A. Wan, "Preparation of tissue engineering porous scaffold with poly(lactic acid) and polyethylene glycol solution blend by solvent-casting/particulate-leaching," *Mater. Res. Express*, vol. 1, no. 4, pp. 0–8, 2015.

[15] K. Kim, M. Yu, X. Zong, J. Chiu, D. Fang, Y. S. Seo, B. S. Hsiao, B. Chu, and M. Hadjiargyrou, "Control of degradation rate and hydrophilicity in electrospun non-woven poly(D,L-lactide) nanofiber scaffolds for biomedical applications," *Biomaterials*, vol. 24, no. 27, pp. 4977–4985, 2003.

[16] Y. Zhang, Z. Wang, F. Jiang, J. Bai, and Z. Wang, "Effect of miscibility on spherulitic growth rate for double-layer polymer films," *Soft Matter*, vol. 9, no. 24, p. 5771, 2013.

[17] Y. Kato, a Boskey, L. Spevak, M. Dallas, M. Hori, and L. F. Bonewald, "Establishment of an osteoid preosteocyte-like cell MLO-A5 that spontaneously mineralizes in culture.," *J. Bone Miner. Res.*, vol. 16, no. 9, pp. 1622–33, 2001.

[18] A. . Stern, M. . Stern, M. . Van Dyke, K. Jähn, M. Prideaux, and L. . Bonewald, "Isolation and culture of primary osteocytes from the long bones of skeletally mature and aged mice," *Biotechniques*, vol. 52, no. 6, pp. 361–373, 2012.

[19] A. Sittichockechaiwut, A. M. Scutt, A. J. Ryan, L. F. Bonewald, and G. C. Reilly, "Use of rapidly mineralising osteoblasts and short periods of mechanical loading to accelerate matrix maturation in 3D scaffolds.," *Bone*, vol. 44, no. 5, pp. 822–9, May 2009.

[20] R. M. Delaine-Smith, S. MacNeil, and G. C. Reilly, "Matrix production and collagen

structure are enhanced in two types of osteogenic progenitor cells by a simple fluid shear stress stimulus," *Eur. Cells Mater.*, vol. 24, no. 0, pp. 162–174, 2012.

[21] M. Sheth, R. A. Kumar, V. Dave, R. A. Gross, and S. P. McCarthy, "Biodegradable polymer blends of poly(lactic acid) and poly(ethylene glycol)," *J. Appl. Polym. Sci.*, vol. 66, no. 8, pp. 1495–1505, 1997.

[22] H. Chen, Y. Liu, Z. Jiang, W. Chen, Y. Yu, and Q. Hu, "Cell-scaffold interaction within engineered tissue," *Exp. Cell Res.*, vol. 323, no. 2, pp. 346–351, 2014.

[23] D. W. Hutmacher, "Scaffold design and fabrication technologies for engineering tissues--state of the art and future perspectives.," *J. Biomater. Sci. Polym. Ed.*, vol. 12, no. 1, pp. 107–124, 2001.

[24] J. S. Park, D. G. Woo, B. K. Sun, H. M. Chung, S. J. Im, Y. M. Choi, K. Park, K. M. Huh, and K. H. Park, "In vitro and in vivo test of PEG/PCL-based hydrogel scaffold for cell delivery application," *J. Control. Release*, vol. 124, no. 1–2, pp. 51–59, 2007.

[25] X. Zhu, T. Zhong, R. Huang, and A. Wan, "Preparation of hydrophilic poly(lactic acid) tissue engineering scaffold via (PLA)-(PLA-b-PEG)-(PEG) solution casting and thermal-induced surface structural transformation," *J. Biomater. Sci. Polym. Ed.*, vol. 26, no. 17, pp. 1286–1296, 2015.

[26] G. Wei and P. X. Ma, "Macroporous and nanofibrous polymer scaffolds and polymer/bone-like apatite composite scaffolds generated by sugar spheres," *J. Biomed. Mater. Res. Part A*, vol. 78A, no. 2, pp. 306–315, 2006.

[27] Y. Chen, S. Zhou, and Q. Li, "Microstructure design of biodegradable scaffold and its effect on tissue regeneration," *Biomaterials*, vol. 32, no. 22, pp. 5003–5014, 2011.

[28] F. J. O'Brien, B. A. Harley, I. V. Yannas, and L. J. Gibson, "The effect of pore size on cell adhesion in collagen-GAG scaffolds," *Biomaterials*, vol. 26, no. 4, pp. 433–441, 2005.

[29] R. Dorati, C. Colonna, I. Genta, T. Modena, and B. Conti, "Effect of porogen on the physico-chemical properties and degradation performance of PLGA scaffolds," *Polym. Degrad. Stab.*, vol. 95, no. 4, pp. 694–701, 2010.

[30] T. M. Freyman, I. V. Yannas, and L. J. Gibson, "Cellular materials as porous scaffolds for tissue engineering," *Prog. Mater. Sci.*, vol. 46, no. 3–4, pp. 273–282, 2001.

Figure Legends

Figure 1: Mean±SD of RR fluorescence for (A) seeding efficiency by comparing day 1 cell attachment on scaffolds and seeding wells. There was no significant difference in seeding efficiency for any scaffold composition (B) increase in metabolic activity over time on each of the scaffold compositions. PLA90 and PLA75 supported significantly higher metabolic activity from day 14 onwards (**=$p<0.01$) (n=6).

Figure 2: Mean±SD for (A) normalized ALP activity on day 14. PLA75 supported significantly higher ALP (**=$p<0.01$) than PLA90 and PLA100. (B) ARS calcium staining on day 21. PLA75 supported significantly more calcium deposition than PLA90 and PLA100 (**=$p<0.01$) (C) DR80 collagen staining on day 21. PLA75 and PLA90 supported significantly higher collagen deposition than PLA100 (*=$p<0.05$) (n=6).

Figure 3: SEM images of scaffolds. (A) shows top surface and cross-sectional views for each scaffold composition (no cells) (B) shows representative images of cell attachment and appearance for each composition. Cells are indicated by a blue arrow. (C) pore size

distribution for each of the scaffold compositions. Pore sizes (μm^2) were analyzed using ImageJ. PLA75 had a larger proportion of large pores and smaller proportion of small pores in comparison to the other two compositions (**=$p<0.01$).

Figure 4: Representative confocal Z-stack images of MLO-A5 cells on each scaffold composition. Nuclei stained with propidium Iodide (PI, red) and actin with phalloidin-FITC (green). Individual channels and composites shown. Control scaffolds were not autofluorescent and therefore appeared black. (For interpretation of the reference to color in this figure legend, the reader is referred to the web version of this article.)
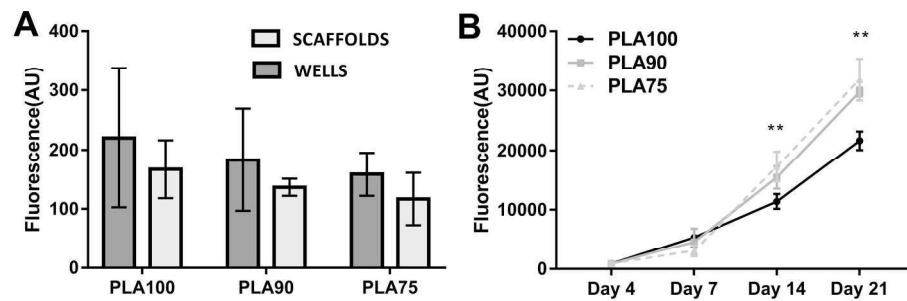
Figure 1. Mean±SD of RR fluorescence for (A) seeding efficiency by comparing day 1 cell attachment on scaffolds and seeding wells. There was no significant difference in seeding efficiency for any scaffold composition (B) increase in metabolic activity over time on each of the scaffold compositions. PLA90 and PLA75 supported significantly higher metabolic activity from day 14 onwards (**=$p < 0.01$) (n=6).
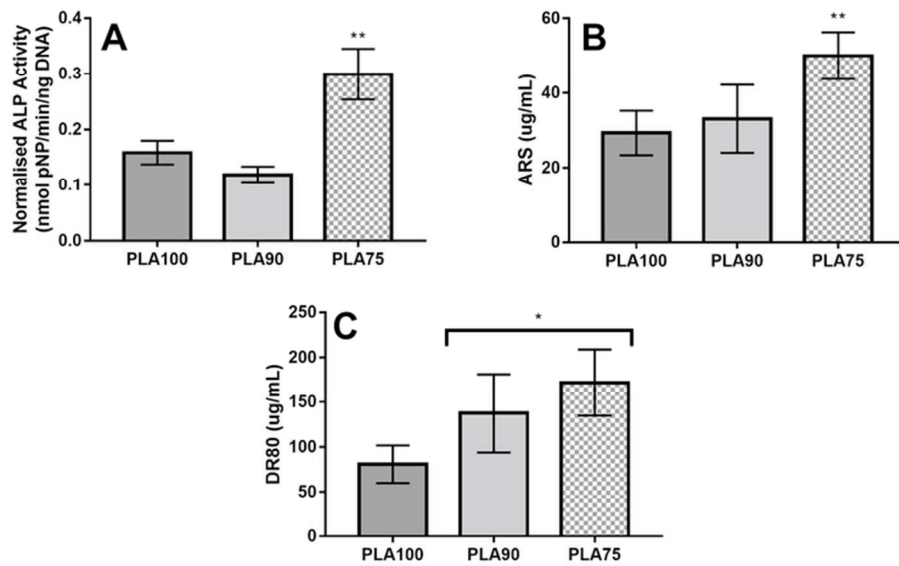
99x35mm (600 x 600 DPI)

Figure 2. Mean±SD for (A) normalized ALP activity on day 14. PLA75 supported significantly higher ALP (**=$p<0.01$) than PLA90 and PLA100. (B) ARS calcium staining on day 21. PLA75 supported significantly more calcium deposition than PLA90 and PLA100 (**=$p<0.01$) (C) DR80 collagen staining on day 21. PLA75 and PLA90 supported significantly higher collagen deposition than PLA100 (*=$p<0.05$) (n=6).
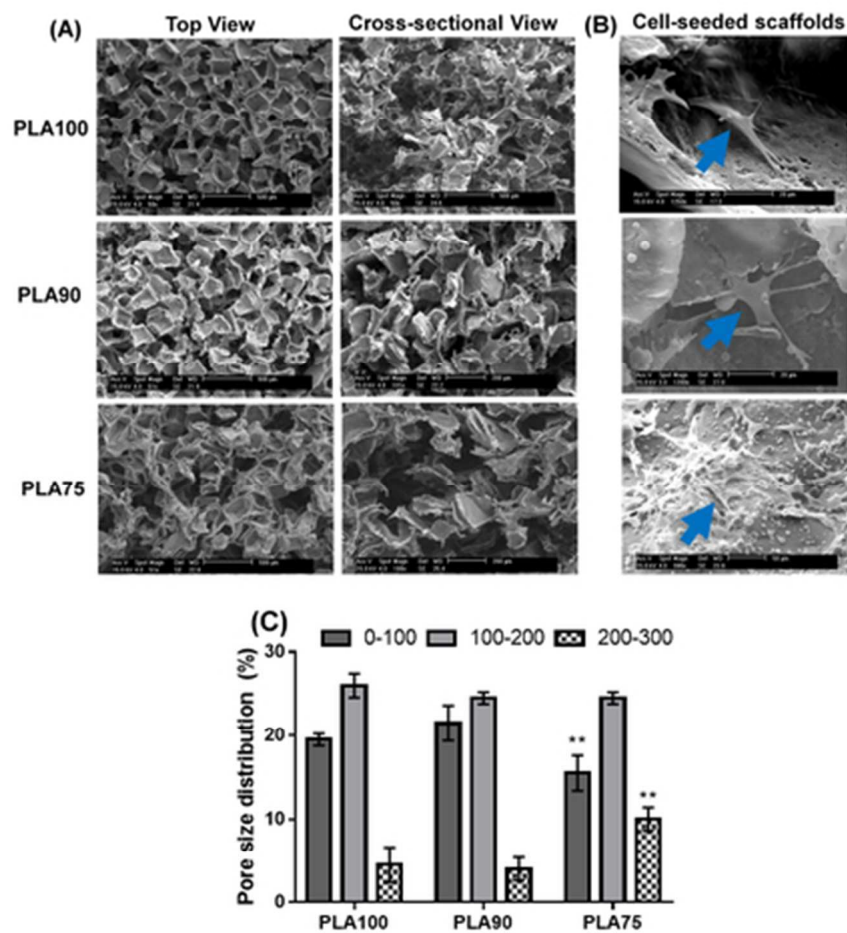
69x44mm (300 x 300 DPI)

Figure 3. SEM images of scaffolds. (A) shows top surface and cross-sectional views for each scaffold composition (no cells) (B) shows representative images of cell attachment and appearance for each composition. Cells are indicated by a blue arrow. (C) pore size distribution for each of the scaffold compositions. Pore sizes (µm2) were analyzed using ImageJ. PLA75 had a larger proportion of large pores and smaller proportion of small pores in comparison to the other two compositions (**=p<0.01).
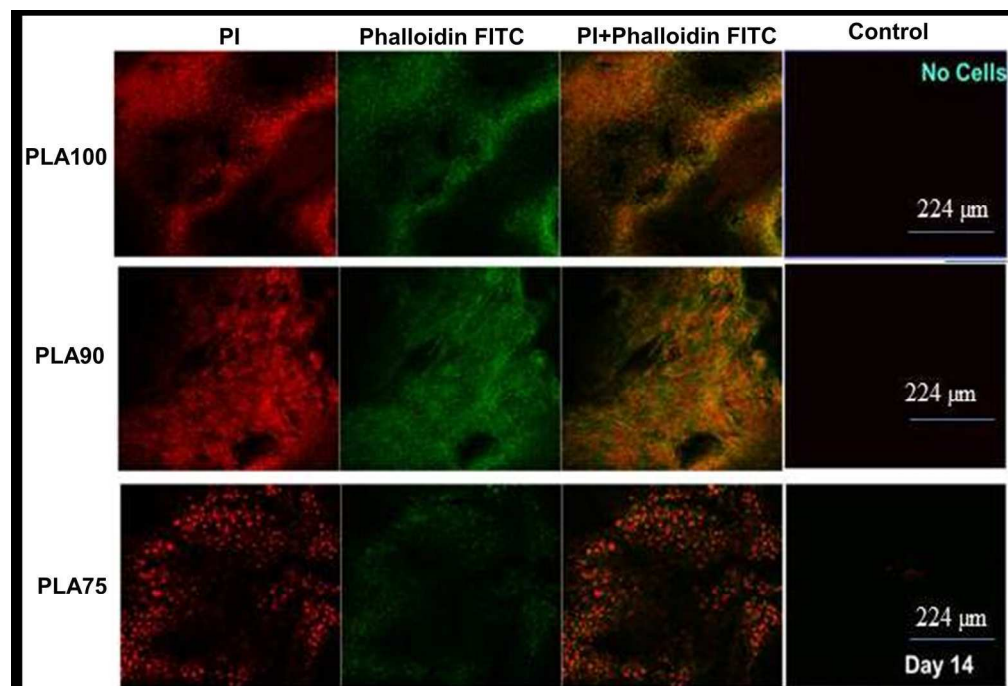
36x41mm (300 x 300 DPI)

Figure 4.Representative confocal Z-stack images of MLO-A5 cells on each scaffold composition. Nuclei stained with propidium Iodide (PI, red) and actin with phalloidin-FITC (green). Individual channels and composites shown. Control scaffolds were not autofluorescent and therefore appeared black. (For interpretation of the reference to color in this figure legend, the reader is referred to the web version of this article.)

182x123mm (300 x 300 DPI)